

Retinotopy Inspired Brain Encoding Model and the All-for-One Training Recipe

Huzheng Yang Jianbo Shi James Gee
 Department of Computer and Information Science
 University of Pennsylvania
 {huze, jshi}@seas.upenn.edu
 gee@upenn.edu

Abstract

Brain encoding models aim to predict brain voxel-wise responses to stimuli images, replicating brain signals captured by neuroimaging techniques. There is a large volume of publicly available data, but training a comprehensive brain encoding model is challenging. The main difficulties stem from a) diversity within individual brain, with functional heterogeneous brain regions; b) diversity of brains from different subjects, due to genetic and developmental differences; c) diversity of imaging modalities and processing pipelines. We use this diversity to our advantage by introducing the All-for-One training recipe, which divides the challenging one-big-model problem into multiple small models, with the small models aggregating the knowledge while preserving the distinction between the different functional regions. Agnostic of the training recipe, we use biological knowledge of the brain, specifically retinotopy, to introduce inductive bias to learn a 3D brain-to-image mapping that ensures a) each neuron knows which image regions and semantic levels to gather information, and b) no neurons are left behind in the model.

We pre-trained a brain encoding model using over one million data points from five public datasets spanning three imaging modalities. To the best of our knowledge, this is the most comprehensive brain encoding model to the date. We demonstrate the effectiveness of the pre-trained model as a drop-in replacement for commonly used vision backbone models. Furthermore, we demonstrate the application of the model to brain decoding. Code and the model checkpoint will be made available.

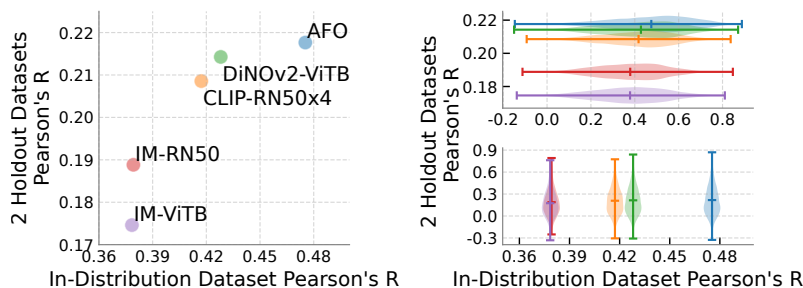


Figure 1: *All-for-One* recipe pre-trained backbone model evaluated by linear probing brain encoding. All models remain frozen, the dimension of latent image features are reduced using PCA to a consistent size. Subsequently, a linear regression is conducted for each voxel. The in-distribution dataset comprises one subject from NSD, the holdout datasets consist of two subjects from BOLD5000 and ThingsfMRI1. Violin plot show distribution of score over voxels.

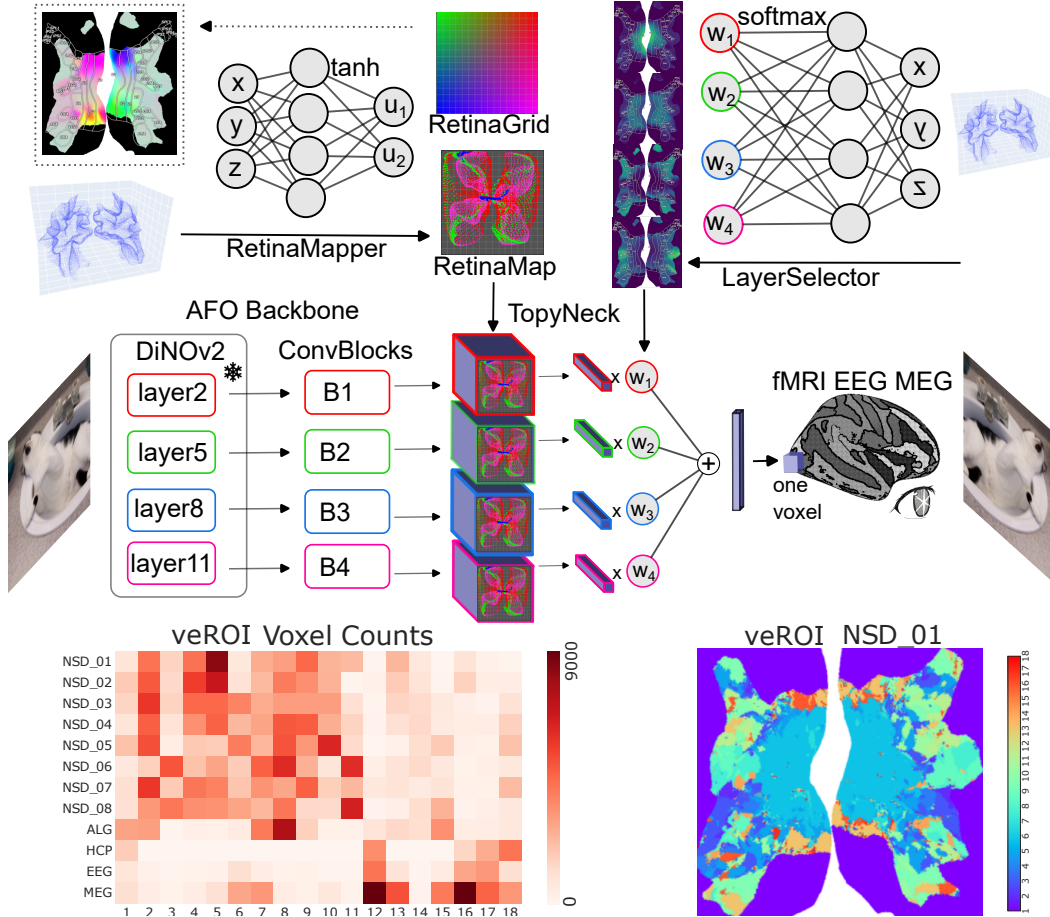


Figure 2: The proposed brain encoding model consists of three main components: the *backbone*, the *TopyNeck*, and the linear regression *head*. The *backbone* is trainable convolution blocks attached to a frozen *DiNOv2-ViT-B* model. *TopyNeck* selects one-dimensional features for each voxel based on its physical coordinates. *TopyNeck* composes of *RetinaMapper* that maps the voxel to a 2D image grid (*RetinaGrid*), and *LayerSelector* that combine feature vectors obtained from backbone layers. Each dot in *RetinaMap* is a voxel, and color corresponds to argmax of *LayerSelector*. Finally, a no-weight-sharing linear regression is conducted for each voxel. Voxel-wise encoding ROI (*veROI*), is a novel brain parcellation that unifies multi-modal subjects.

1 Introduction

There is a growing body of research in neuroscience that utilizes brain encoding models. The model predicts voxel-wise brain response to visual stimuli, and it can be depicted as a multi-task regression problem where each voxel is a task. The brain encoding model serves as a computational counterpart to biological brains [29]. The common practice for building brain encoding models is to use pre-trained models from image classification [6], text-to-image alignment [23], or self-supervised tasks [21]. These pre-trained models may excel at their benchmarked task; however, [25] show that the image-classification benchmark score does not align with prediction performance in brain encoding.

Building a model from all data sources poses a significant challenge due to heterogeneity in data: a) diversity in functional sub-modules within each brain, b) genetic and developmental differences across subjects, c) inconsistent imaging techniques and pre-processing pipelines. The current best practice is to build Region-of-Interest (ROI)¹ models over subjects from the same dataset [4] [30] [1], where ROIs are predefined by well-studied anatomical and functional properties of the brain voxels. However, the ROI-model approach lacks the potential benefits for ROIs to aggregate knowledge and collaborate. This issue can be mitigated to some extent by adjusting the granularity of ROIs. This work proposes a multi-stage All-for-One (AFO) training recipe that explicitly lets ROIs aggregate

¹ROI refers to brain atlas parcellations

knowledge while keeping the main training objective less challenging than training for one all-ROI model. Borrowing the idea of ‘Dark knowledge’ distillation [13], we use denoising to ensure the aggregated knowledge is clean.

Biological domain knowledge of the brain, specifically retinotopy, can be explored to design a better model [19]. The retina cells are physically wired through the optic nerve to the lateral geniculate nucleus, which connects to the visual cortex. Thus, visual cortex cells preserve the topological structure of images projected to the retina. This study explicitly defines a *RetinaMapper* function that replicates retinotopic mapping. An obvious solution is learning a forward mapping that transforms 2D *RetinaGrid* into a neuron in a 3D brain location. However, such forward mapping can not guarantee to be surjective: every 3D neuron location is the mapped from at least one 2D *RetinaGrid*. Our solution is to model the *RetinaMapper* from the inverse perspective, mapping 3D neuron to 2D *RetinaGrid*. *RetinaMapper* is learned without ground-truth supervision, but still exhibits retinotopic behavior, as shown in our results.

A well-reported phenomenon is that neuron voxels are mapped to shallow to deep layers of a feed-forward neuron network [27]. This motivates the common practice of selecting the best layers for each voxel. But per-voxel hyper-parameter tuning is highly noisy and prone to overfitting; previous studies overcome this by choosing the same layers for each ROI. In this study, we propose a *LayerSelector* module that enforces spatial proximity, thus allowing a flexible and robust selection of layers.

2 Related work

The field of computational neuroscience has been actively exploring the task of brain encoding, highlighting from [15] [20], surveyed by [29]. There are several initiatives and benchmarks: The brain-score [25] initiative compares frozen image backbone models using a PCA and linear regression pipeline. The PCA approach allows for a fair comparison of vision models with different latent dimensions. Additionally, [5] utilized a similar frozen PCA pipeline to benchmark various vision models on the NSD dataset. The Algonauts challenge [4] benchmarks end-to-end trained model without the constraint of frozen model and PCA dimension reduction. The Sensorium benchmark [30] worked on invasive mouse V1 imaging data. The Things initiative [12] provides fine-grid image captions which can be used for hypotheses testing. These datasets and benchmarks cover a wide range of imaging modalities, and preprocessing and denoising pipelines [16] [22]. The All-for-One training recipe aims to leverage all of these diverse data sources to pre-train a comprehensive brain encoding model.

The neuroscience community has extensively applied brain encoding models to unravel the biological mechanisms underlying brain function. [26] employed transfer learning techniques with brain encoding models to investigate the hierarchical organization of the brain. [8] applied the model to study color coding in mouse neurons. The NeuroGen framework [10] combined brain encoding models with image generation models, they utilize gradient-based methods to manipulate stimulus images. [2] generated maximally excited images for populations of neurons and presented these images to subjects to validate the conclusions. On the other hand, there are fruitful studies of brain decoding² without a brain encoding model [27] [11] [18] [11]. Their framework is to take a pre-trained text-conditioned image generation model [14] [24], then train a mapping function that aligns brain patterns to the text-condition embeddings space. However, we argue that decoding without a pre-trained encoding model is less efficient: Firstly, this pipeline is tightly linked to the pre-trained image generation model. Also, this pipeline face challenges in effectively utilizing heterogeneous data from various imaging modalities. We argue that decoding with a frozen encoding model is more efficient as this approach is agnostic to the specific image generation model.

Previous studies also explored incorporating retinotopy into the brain encoding model. [1] fits Gabor filters of various sizes and locations for each voxel. [19] also employed the *RetinaMapper*, but their work focuses on training with the same imaging modality and one single ROI. In contrast, our approach tries to model the whole visual brain with diverse data sources.

²We use the term *encoding* for mapping from stimuli image to brain voxels, *decoding* for the reverse.

3 Method

The voxel-wise encoding model (Fig 2) comprises three main components: Firstly, the **backbone** processes the input image and extracts latent image features from its intermediate layers. Next, the **neck** component compresses the feature vector for each voxel. Finally, the **head** applies a linear regression model to fit a prediction for each voxel. Let $M^l \in \mathcal{R}^{D \times \frac{H}{k} \times \frac{W}{k}}$ be the feature map output from the frozen backbone, where l is the layer index, k is the down-scale factor, we refer the $\frac{H}{k} \times \frac{W}{k}$ grid as *RetinaGrid*. The brain encoding model can be formulated as learning a mapping function \mathcal{F} (Eq 1), where \mathcal{N} depends on the imaging modality³. $\mathcal{N}_{MRI} := (X \times Y \times Z) \times 1$, $\mathcal{N}_{EEG} := C \times T$, $\mathcal{N}_{MEG} := (X \times Y \times Z) \times T$

$$\mathcal{F} : \mathcal{R}^{(L \times D) \times \frac{H}{k} \times \frac{W}{k}} \rightarrow \mathcal{R}^{\mathcal{N}} \quad (1)$$

3.1 TopyNeck

RetinaMapper The biological retinotopy process is mapping $f : \mathcal{R}^{\frac{H}{k} \times \frac{W}{k}} \rightarrow \mathcal{R}^{X \times Y \times Z}$. *RetinaMapper* aims to replicate this mapping. However, f can not guarantee to be surjective: every 3D neuron location is the mapped from at least one 2D *RetinaGrid*. Instead of the forward mapping f , we learn a reverse injective mapping $f' : \mathcal{R}^{X \times Y \times Z} \rightarrow \mathcal{R}^{\frac{H}{k} \times \frac{W}{k}}$ and use \tanh activation function to guarantee the output 2D coordinates lies within the *RetinaGrid*. The *RetinaMapper* is formulated as

$$u = \tanh(\text{MLP}(\text{PE}(p))) \quad (2)$$

where $p \in \mathcal{R}^{\mathcal{N} \times 3}$ is the voxel’s spatial coordinate, PE is sinusoidal positional encoding function, $u \in \mathcal{R}^{\mathcal{N} \times 2}$ is coordinates in the *RetinaGrid*. During training, a small non-trainable variance σ is introduced $u' \sim \mathcal{N}(u, \sigma)$. At inference time σ is set to 0. At each u' , linear interpolation is performed to obtain a 1-D feature vector $m^l \in \mathcal{R}^{\mathcal{N} \times D}$ for each layer l . Furthermore, Another 1-D feature vector $q^l = \text{MLP}(\text{GlobalAvgPool}(M^l), \text{GlobalMaxPool}(M^l))$ is added to m^l . Parameters of *RetinaMapper* is shared for all layers. Figure 2 and 4 show examples of such mapping. The color dots in *RetinaGrid* indicate which 3D neuron layers it is from. The blank area indicates image regions that are unused for prediction.

LayerSelector Early visual to downstream regions have growing receptive field sizes and neurons’ latent representation of the stimuli image grows abstract. This motivates matching voxels to layers in feed-forward neuron networks. But selecting the best or top layers for each voxel is suspected to be overfitting. *LayerSelector* enforce spatial proximity formulated as

$$\eta = \text{softmax}(\text{MLP}(\text{PE}(p))) \quad (3)$$

where $\eta \in \mathcal{R}^{\mathcal{N} \times L}$. The 1-D feature vectors sampled from various layers at *RetinaGrid* is reduced as $m_i^* = \sum_L \eta_i^l m_i^l$. Regularization loss $l_{ent} = \sum_L \eta^l \log \eta^l$ is applied to prevent converging to a local minimum that only selects one single layer.

3.2 All-for-One training recipe

Dividing neuron voxels into ROIs loses ROIs’ potential to aggregate knowledge and collaborate. Mixing can also negatively affect individual voxel performance, making learning more challenging. The AFO recipe aims to gather the benefits from both dividing and mixing. Multiple stages models are trained (Figure 3): In stage one, each ROI model is trained separately. In stage two, each ROI model is trained to distill the dark knowledge [13] from all other ROIs, but the ground truth loss is only applied on the target ROI, other ROIs are helpers, and their parameters were discarded after training. Model checkpointing and early stopping are conditioned only on the target ROI. In stage three, the final model is trained with all ROIs as outputs, with dark knowledge and ground truth loss. The final product is one comprehensive all-ROI model.

³We use a unified term *voxel* to refer to a single smallest element in \mathcal{N} .

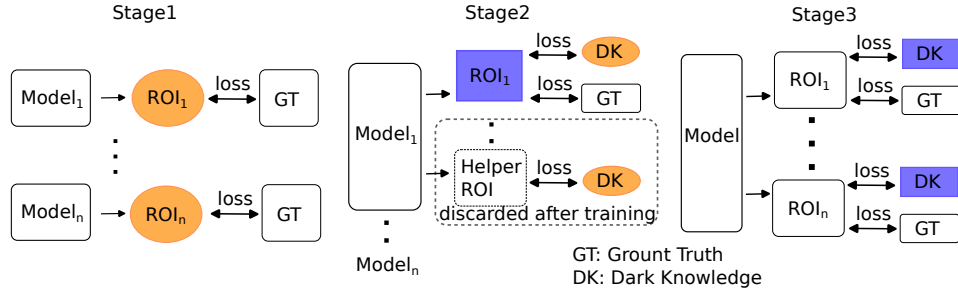


Figure 3: *All-for-One* training recipe involves training multiple stage of models using dark knowledge distillation. In **Stage1**, a separate model is trained for each ROI. In **Stage2**, each model is an all-ROI model that leverages the dark knowledge from all other models as helpers, the parameters of these helper models are discarded after training. In **Stage3**, a single all-ROI model is trained.

Table 1: Brain encoding datasets. The term *Datapoints* refers to the number of image stimulus presentations, including repeated presentation of the same image.

	Training Datasets					Holdout Datasets	
	NSD	HCP MOVIE	Algonauts 2021	Things MEG1	Things EEG2	BOLD 5000	Things fMRI1
Datapoints	240K	441K	30K	88K	640K	20K	24K
Subjects	8	184	10	4	10	4	3
Voxels	315K	29K	13K	60K	17K	9K	19K
Modality	7T fMRI	7T fMRI	3T fMRI	MEG	EEG	3T fMRI	3T fMRI

3.3 Voxel-wise encoding ROI

We need a unified ROI parcellation that is defined for all subjects from various imaging modalities. To generate such a unified ROI, we utilize the final linear regression weight, which is extracted from an average of 10 all-ROI models. We start by performing Euclidean distance k-means clustering on the weights to reduce the dimension of voxel counts. Subsequently, Ward’s method applies hierarchical clustering to find the cluster centroids. This hierarchical clustering results in a dendrogram. We cut the dendrogram at a hand-picked threshold to identify the *veROIs*. By adjusting this threshold, we can control the granularity of the *veROIs*.

4 Experiments

4.1 Datasets

We utilize 7 publicly available datasets for our experiments (Table 1). Details are provided in [1] [28] [4] [12] [9] [3]. We use only voxels from the visual brain. Each dataset was divided into training, validation, and test sets with a ratio around 90 : 6 : 4. We use repetition-averaged brain response. For the Things datasets, we use repeatedly represented images as the test set. All the experiment results are reported from the test set unless specified. The HCP video was split into chunks of 20 seconds to ensure no data leak, and a time delay of 4 seconds between video frames and fMRI frames was applied [17], blank resting-state segments are not discarded. For video stimulus, we extracted frames at a rate of one frame per second. We only use one frame for the ALG dataset.

Notably, except for the NSD dataset, all subjects from other datasets viewed the same set of images. As a compromise for computation intensity, we concatenated the voxels from ALG EEG MEG subjects into each single large brain, voxel’s spatial coordinates are placed in an evenly spaced grid. For the HCP dataset, a group average was performed due to the large number of subjects and the lower SNR in each individual subject. All datasets have spatial coordinates for voxels except the EEG dataset, EEG voxel’s spatial coordinates are generated from dummy sequential numbers.

4.2 TopyNeck probing

RetinaMapper In Figure 4, for NSD subjects, early visual voxels were mapped to span most of the *RetinaGrid*, while downstream-region voxels remained concentrated in the center. The ablation study presented in Table 2 further demonstrates the outstanding importance of the *RetinaMapper* for early visual voxels in NSD subjects. This alignment with retinotopy design motivation. However, for other low SNR datasets, no clear retinotopic mapping was observed, suggesting that the *RetinaMapper* may not be necessary in such cases, and a constant mapping to the center could be sufficient.

LayerSelector In Figure 5, for subject NSD_01, a smooth transition from shallow to deep layers was observed. This alignment with the design motivation. Ablation study in Table 2 also indicates significant improvement for NSD subjects compared to un-weighted averaging layers or selecting a single layer. However, for low SNR datasets, the trend was to select only the last layer (Figure 4), suggesting that the *LayerSelector* module may not be necessary in such cases.

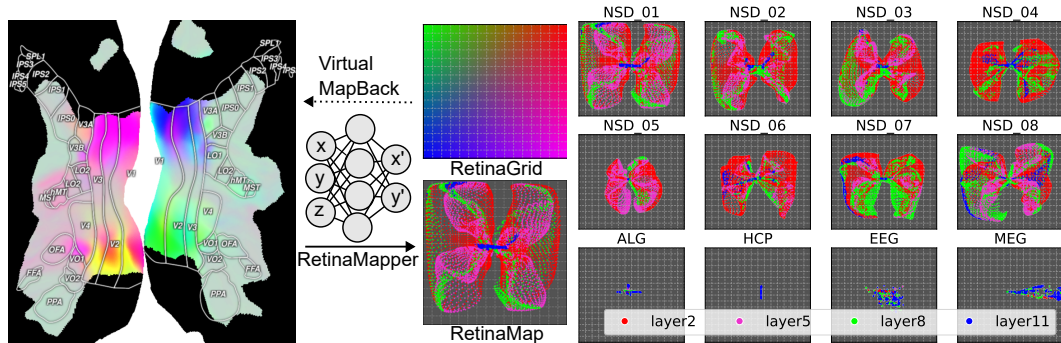


Figure 4: *RetinaMapper* maps voxels to *RetinaGrid*. Each dot on *RetinaMap* is a voxel colored by argmax of the *LayerSelector*, colors indicate selection of layers.

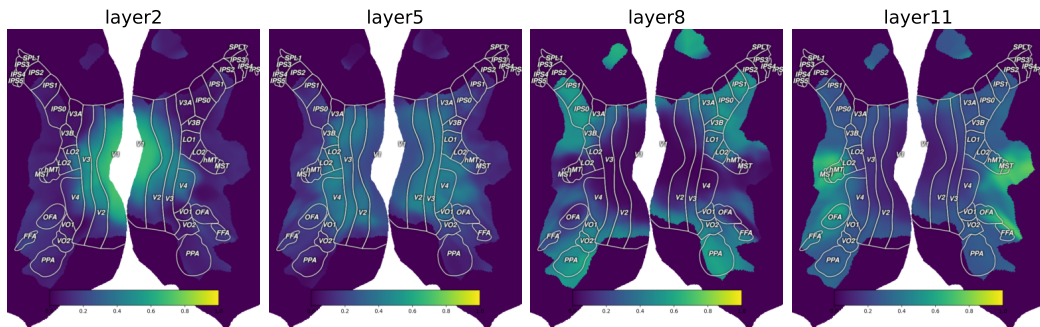


Figure 5: *LayerSelector* re-weights backbone layers, outputs for all layers sum to 1. Results are shown for subject NSD_01.

4.3 All-for-One recipe results

In Table 3, a significant performance gap between the S1 and S2 models indicates the effectiveness of aggregating knowledge among ROIs. We also study a randROI that has the exact same number of ROIs and number of voxels inside each ROI. S1 and S2 gap is not observed in the randROI approach, as randROI already covers all types of voxels in every ROI. Furthermore, the model trained with ground truth (NoDK) as helpers shows little to no improvement over the S1 model. This suggests that the quality of the helper ROI is critical for the AFO recipe, as involving noisy helpers makes the training process unnecessarily challenging. In this context, dark knowledge plays a crucial role as

Table 2: *TopyNeck* ablation study. The reported numbers are the average Pearson correlation coefficient across all voxels. Results are averaged over three runs. *FrozenRM* maps every voxel to the center, *FrozenLS* outputs uniform weight for each layer. *NoRegLS* selects a single layer.

Subject	NSD_01				NSD_08				EEG
	all	early	late	mid	all	early	late	mid	all
FullTopyNeck	0.462	0.515	0.435	0.470	0.291	0.304	0.285	0.292	0.228
FrozenRM	<u>0.441</u>	<u>0.476</u>	0.422	<u>0.452</u>	<u>0.274</u>	<u>0.261</u>	0.280	<u>0.272</u>	0.226
w/o GlobalPool	0.457	0.513	0.428	0.467	0.293	0.303	0.289	0.295	0.230
FrozenLS	0.451	0.512	0.419	0.466	0.280	0.300	<u>0.270</u>	0.279	<u>0.224</u>
NoRegLS	0.447	0.505	<u>0.417</u>	0.464	0.287	0.299	0.282	0.284	0.229

Table 3: *All-for-One* training recipe ablation study. The reported numbers are the average Pearson correlation coefficient across all voxels, NSD(NC) is the median of noise-normalized score. *NaiveMix* train one all-ROI model. *NoDK* use ground truth as helpers. *randROI* and *veROI* has the exact same size. *S2+1* indicates one extra iteration of stage2. *b* is number of parameters in the convolution blocks, *n* is number of voxels, *d* is feature dimension, *r* is number of ROIs.

Method	# Params	Dataset(s)						
		NSD	EEG	MEG	HCP	ALG	ALL	NSD (NC)
NaiveMix	$b + nd$	<u>0.422</u>	<u>0.212</u>	<u>0.180</u>	<u>0.340</u>	<u>0.256</u>	<u>0.367</u>	<u>0.560</u>
veROIS1	$rb + nd$	0.425	<u>0.212</u>	0.194	0.346	0.265	0.371	0.567
veROIS2	$rb + nd$	0.433	0.222	0.209	0.365	0.266	0.380	0.588
veROIS3	$b + nd$	0.435	0.225	0.210	0.366	0.267	0.382	0.593
veROIS2+1	$rb + nd$	0.432	0.226	0.211	0.362	0.264	0.380	0.586
NoDK	$rb + nd$	0.426	0.216	0.186	0.349	<u>0.256</u>	0.371	0.569
randROIS1	$rb + nd$	0.431	0.216	0.207	0.343	0.258	0.377	0.584
randROIS2	$rb + nd$	0.432	0.220	0.207	0.348	0.259	0.378	0.586

denoising. However, solely dark knowledge distillation doesn't have a great impact as can be inferred from the small gap between randROI S1 and S2 models.

4.4 veROI results

Figure 6 shows veROI on cortex across all NSD subjects, early visual areas is centered around veROI_5 (blue) and downstream areas centered around veROI_9 (green), voxels that drop out from the field of view in early visual areas are centered around veROI_16 (red). The score for each veROI for subject NSD_01 can be found in Figure 8, where veROI_12 onward is mainly for the low SNR voxels. From the heatmap in Figure 2 we can also observe that veROI_12 onward is mainly HCP, EEG, and MEG subjects.

4.5 Brain decoding

Methods In this study, brain decoding refers to the task of ranking and retrieving candidate images from a candidate set, retrieved images are to match a given brain response pattern. The decoding pipeline involves forwarding each candidate image through the brain encoding model and measuring Pearson's correlation coefficient between the model's prediction and the ground truth.

Results The experiments are conducted on 500 validation images as candidate images. As a qualitative analysis, Figure 7 and Figure 9 demonstrate that when conditioning on the early visual area or veROI_5, texture and orientation are more preserved in the decoded images. Conversely,

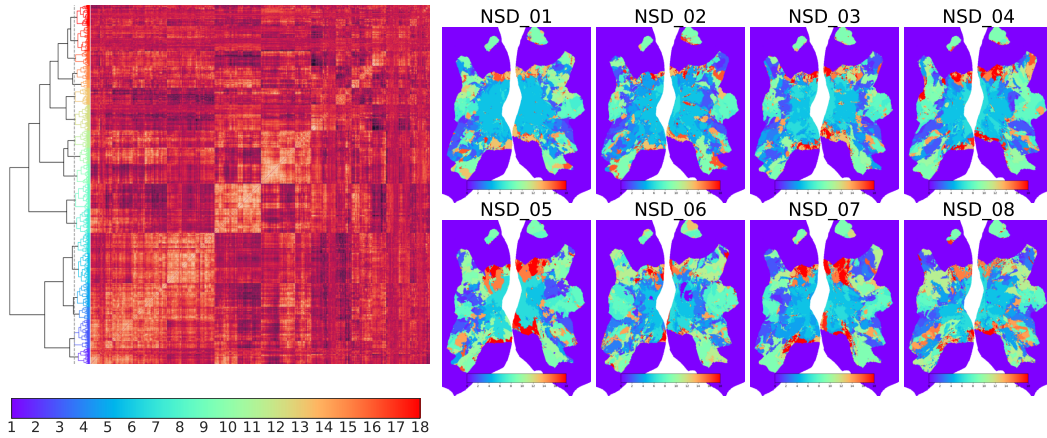


Figure 6: *veROI* cluster voxels into ROIs by hierarchical clustering. ROIs are identified by cutting the linkage at a manually selected threshold value(dashed line). The feature used for clustering is the linear regression weight associated with each voxel.

when conditioning on downstream ROIs, semantic concepts are more preserved. Additionally, Figure 8 shows that image retrieval achieves high accuracy when conditioned on early ROIs. Quantitative exploration of the functional roles of ROIs is beyond the scope of this study. Future work may involve investigating semantic concepts with image generation models. Furthermore, the gradient of the encoding model can be utilized to facilitate image generation and manipulation.

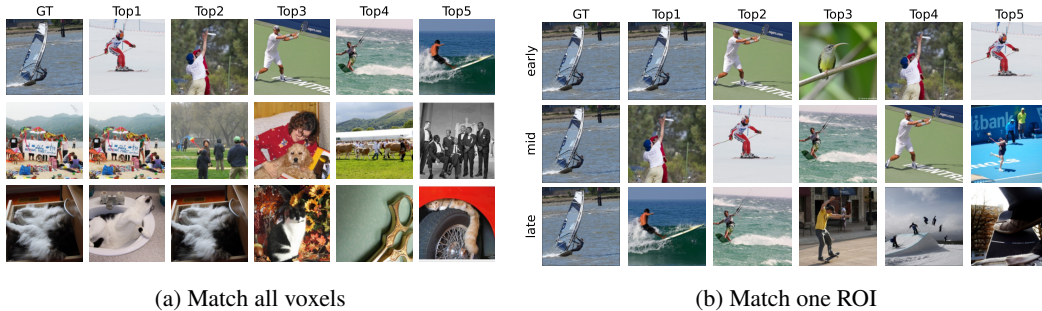


Figure 7: Image retrieval to match brain response pattern. Images are ranked by Pearson's r of captured biological brain pattern and model output. Results are for subject NSD_01.

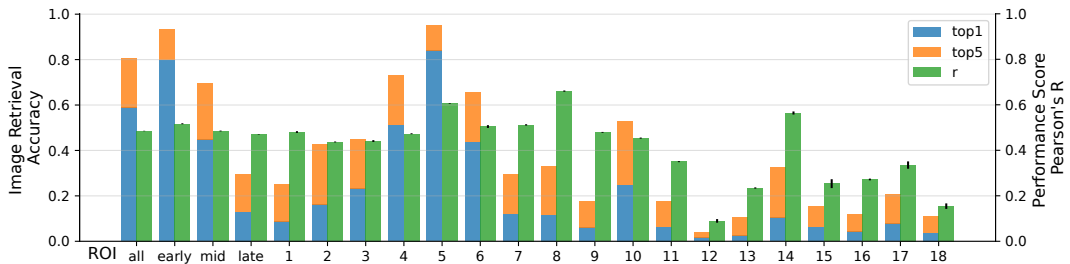


Figure 8: Performance of image retrieval(blue and orange) conditioned on ROIs. The integer numbers are the indices of the *veROIs*. Performance scores of brain encoding(green) are the average value of the voxels within each ROI, standard error is in black. Results are for subject NSD_01.



Figure 9: Image retrieval conditioned on *veROIs*. The numerical numbers are the indices of *veROIs*. The top four images are placed from the top left to the bottom right.

4.6 Implementation details

We use smooth L1 loss with $\beta = 0.01$, regularization loss l_{ent} is scaled down by $\lambda = 0.00003$. AdaBelief optimizer [32] is employed with `lr = 0.003`, `batchsize = 128`, `weight_decay = 0.0001`, $(\beta_1, \beta_2) = (0.9, 0.999)$. Notably, we mix subjects in one mini-batch, and the effective batch size for each subject is less than the total. Due to memory constrain, we randomly sample up to 8000 voxels for each training datapoint, there is 436,715 voxels totaling all subjects. Early stopping is configured with `patience = 20` epochs, we define one epoch as 10% of the total training data. Greedy *Model Soup* [31] is applied at the top 10 validation checkpoints. Backbone is kept frozen except `LayerNorm` running statistics is updated. Input resolution is 224×224 and the feature from backbone layers are all of the size $768 \times 16 \times 16$. The attached trainable convolution block is three zero-padded 5×5 convolutions with skip connection and `LayerNorm`, $C = 768$. The last convolution layer reduces the dimension to $D = 256$. We trained all models on single NVIDIA RTX 2080 Ti 12GB GPUs at a reduced clock speed of 1140Mhz, single-subject all-ROI models consume half to 1 GPU hour, all-subject single-ROI models consume 3 to 5 GPU hours, all-subject all-ROI models consume 10 GPU hours. The complete AFO recipe total around 300 GPU hours. Models are trained Pytorch Lightning [7] mixed precision FP16. To boost training speed, MLPs in *RetinaMapper* and *LayerSelector* are pre-optimized by a single-subject all-ROI model, they are loaded and kept frozen in the AFO recipe, this gives 2 times faster convergence speed.

5 Conclusion and Limitations

We proposed the *AFO* recipe alongside *veROI* to address the issue of heterogeneity in publicly available datasets. To the best of our knowledge, our pre-trained model constructed with over 1 million data points is the most comprehensive brain encoding model to date. The model shows superior performance when transferred to small hold-out datasets. As demonstrated by our brain decoding experiments, the pre-trained model could facilitate further neuroscience research.

We designed *TopyNeck* inspired by retinotopy, which showed retinotopic behavior despite having no ground truth supervision for the retinotopic mapping function. However, the retinotopic behavior diminishes when the target dataset SNR is low, e.g. EEG, MEG. This suggests a simple alternative approach is sufficient in such a case.

A fundamental limitation for this study is that: we use repetition-averaged brain response as prediction target, this is a common simplification that assume brain response from each repetition is consistent. However, this fundamental assumption is not true if we consider: 1. memory state that depends on previously presented images. 2. brain state which depends on the time of the day and relative time of each scanning session. 3. behavior response such as button press. 4. gaze pattern captured by eye tracking camera or eye voxels.

References

- [1] Emily J. Allen, Ghislain St-Yves, Yihan Wu, Jesse L. Breedlove, Jacob S. Prince, Logan T. Dowdle, Matthias Nau, Brad Caron, Franco Pestilli, Ian Charest, J. Benjamin Hutchinson, Thomas

- Naselaris, and Kendrick Kay. A massive 7T fMRI dataset to bridge cognitive neuroscience and artificial intelligence. *Nature Neuroscience*, 25(1):116–126, January 2022. ISSN 1546-1726. doi: 10.1038/s41593-021-00962-x. URL <https://www.nature.com/articles/s41593-021-00962-x>. Number: 1 Publisher: Nature Publishing Group.
- [2] Pouya Bashivan, Kohitij Kar, and James J. DiCarlo. Neural population control via deep image synthesis. *Science*, 364(6439):eaav9436, May 2019. doi: 10.1126/science.aav9436. URL <https://www.science.org/doi/abs/10.1126/science.aav9436>. Publisher: American Association for the Advancement of Science.
- [3] Nadine Chang, John A. Pyles, Austin Marcus, Abhinav Gupta, Michael J. Tarr, and Elissa M. Aminoff. BOLD5000, a public fMRI dataset while viewing 5000 visual images. *Scientific Data*, 6(1):49, May 2019. ISSN 2052-4463. doi: 10.1038/s41597-019-0052-3. URL <https://www.nature.com/articles/s41597-019-0052-3>. Number: 1 Publisher: Nature Publishing Group.
- [4] R. M. Cichy, K. Dwivedi, B. Lahner, A. Lascelles, P. Iamshchinina, M. Graumann, A. Andonian, N. A. R. Murty, K. Kay, G. Roig, and A. Oliva. The Algonauts Project 2021 Challenge: How the Human Brain Makes Sense of a World in Motion, April 2021. URL <http://arxiv.org/abs/2104.13714>. arXiv:2104.13714 [cs, q-bio].
- [5] Colin Conwell, Jacob S. Prince, George A. Alvarez, and Talia Konkle. Large-Scale Benchmarking of Diverse Artificial Vision Models in Prediction of 7T Human Neuroimaging Data, March 2022. URL <https://www.biorxiv.org/content/10.1101/2022.03.28.485868v1>. Pages: 2022.03.28.485868 Section: New Results.
- [6] Jia Deng, Wei Dong, Richard Socher, Li-Jia Li, Kai Li, and Li Fei-Fei. ImageNet: A large-scale hierarchical image database. In *2009 IEEE Conference on Computer Vision and Pattern Recognition*, pages 248–255, June 2009. doi: 10.1109/CVPR.2009.5206848. ISSN: 1063-6919.
- [7] William A. Falcon. Pytorch lightning. *GitHub*, 3, 2019.
- [8] Katrin Franke, Konstantin F. Willeke, Kayla Ponder, Mario Galdamez, Na Zhou, Taliah Muhammad, Saumil Patel, Emmanouil Froudarakis, Jacob Reimer, Fabian H. Sinz, and Andreas S. Tolias. State-dependent pupil dilation rapidly shifts visual feature selectivity. *Nature*, 610(7930):128–134, October 2022. ISSN 1476-4687. doi: 10.1038/s41586-022-05270-3. URL <https://www.nature.com/articles/s41586-022-05270-3>. Number: 7930 Publisher: Nature Publishing Group.
- [9] Alessandro T. Gifford, Kshitij Dwivedi, Gemma Roig, and Radoslaw M. Cichy. A large and rich EEG dataset for modeling human visual object recognition. *NeuroImage*, 264:119754, December 2022. ISSN 1053-8119. doi: 10.1016/j.neuroimage.2022.119754. URL <https://www.sciencedirect.com/science/article/pii/S1053811922008758>.
- [10] Zijin Gu, Keith Wakefield Jamison, Meenakshi Khosla, Emily J. Allen, Yihan Wu, Ghislain St-Yves, Thomas Naselaris, Kendrick Kay, Mert R. Sabuncu, and Amy Kuceyeski. NeuroGen: Activation optimized image synthesis for discovery neuroscience. *NeuroImage*, 247:118812, February 2022. ISSN 1053-8119. doi: 10.1016/j.neuroimage.2021.118812. URL <https://www.sciencedirect.com/science/article/pii/S1053811921010831>.
- [11] Zijin Gu, Keith Jamison, Amy Kuceyeski, and Mert Sabuncu. Decoding natural image stimuli from fMRI data with a surface-based convolutional network, March 2023. URL <http://arxiv.org/abs/2212.02409>. arXiv:2212.02409 [cs, q-bio].
- [12] Martin N Hebart, Oliver Contier, Lina Teichmann, Adam H Rockter, Charles Y Zheng, Alexis Kidder, Anna Corriveau, Maryam Vaziri-Pashkam, and Chris I Baker. THINGS-data, a multi-modal collection of large-scale datasets for investigating object representations in human brain and behavior. *eLife*, 12:e82580, February 2023. ISSN 2050-084X. doi: 10.7554/eLife.82580. URL <https://doi.org/10.7554/eLife.82580>. Publisher: eLife Sciences Publications, Ltd.
- [13] Geoffrey Hinton, Oriol Vinyals, and Jeff Dean. Distilling the Knowledge in a Neural Network, March 2015. URL <http://arxiv.org/abs/1503.02531>. arXiv:1503.02531 [cs, stat].
- [14] Jonathan Ho, Ajay Jain, and Pieter Abbeel. Denoising Diffusion Probabilistic Models, December 2020. URL <http://arxiv.org/abs/2006.11239>. arXiv:2006.11239 [cs, stat].

- [15] Kendrick N. Kay, Thomas Naselaris, Ryan J. Prenger, and Jack L. Gallant. Identifying natural images from human brain activity. *Nature*, 452(7185):352–355, March 2008. ISSN 0028-0836, 1476-4687. doi: 10.1038/nature06713. URL <http://www.nature.com/articles/nature06713>.
- [16] Kendrick N. Kay, Ariel Rokem, Jonathan Winawer, Robert F. Dougherty, and Brian A. Wandell. GLMdenoise: a fast, automated technique for denoising task-based fMRI data. *Frontiers in Neuroscience*, 7, 2013. ISSN 1662-453X. doi: 10.3389/fnins.2013.00247. URL <http://journal.frontiersin.org/article/10.3389/fnins.2013.00247/abstract>.
- [17] Meenakshi Khosla, Gia H. Ngo, Keith Jamison, Amy Kuceyeski, and Mert R. Sabuncu. Cortical response to naturalistic stimuli is largely predictable with deep neural networks. *Science Advances*, 7(22):eabe7547, May 2021. ISSN 2375-2548. doi: 10.1126/sciadv.abe7547.
- [18] Yizhuo Lu, Changde Du, Dianpeng Wang, and Huiguang He. MindDiffuser: Controlled Image Reconstruction from Human Brain Activity with Semantic and Structural Diffusion, March 2023. URL <http://arxiv.org/abs/2303.14139>. arXiv:2303.14139 [cs].
- [19] Konstantin-Klemens Lurz, Mohammad Bashiri, Konstantin Willeke, Akshay Jagadish, Eric Wang, Edgar Y. Walker, Santiago A. Cadena, Taliah Muhammad, Erick Cobos, Andreas S. Tolias, Alexander S. Ecker, and Fabian H. Sinz. Generalization in data-driven models of primary visual cortex. January 2021. URL <https://openreview.net/forum?id=Tp7kI90Htd>.
- [20] Thomas Naselaris, Kendrick N. Kay, Shinji Nishimoto, and Jack L. Gallant. Encoding and decoding in fMRI. *NeuroImage*, 56(2):400–410, May 2011. ISSN 10538119. doi: 10.1016/j.neuroimage.2010.07.073. URL <https://linkinghub.elsevier.com/retrieve/pii/S1053811910010657>.
- [21] Maxime Oquab, Timothée Darcet, Théo Moutakanni, Huy Vo, Marc Szafraniec, Vasil Khalidov, Pierre Fernandez, Daniel Haziza, Francisco Massa, Alaaeldin El-Nouby, Mahmoud Assran, Nicolas Ballas, Wojciech Galuba, Russell Howes, Po-Yao Huang, Shang-Wen Li, Ishan Misra, Michael Rabbat, Vasu Sharma, Gabriel Synnaeve, Hu Xu, Hervé Jegou, Julien Mairal, Patrick Labatut, Armand Joulin, and Piotr Bojanowski. DINOv2: Learning Robust Visual Features without Supervision, April 2023. URL <http://arxiv.org/abs/2304.07193>. arXiv:2304.07193 [cs].
- [22] Jacob S. Prince, Ian Charest, Jan W. Kurzwski, John A. Pyles, Michael J. Tarr, and Kendrick N. Kay. Improving the accuracy of single-trial fMRI response estimates using GLMsingle. *eLife*, 11:e77599, November 2022. ISSN 2050-084X. doi: 10.7554/eLife.77599.
- [23] Alec Radford, Jong Wook Kim, Chris Hallacy, Aditya Ramesh, Gabriel Goh, Sandhini Agarwal, Girish Sastry, Amanda Askell, Pamela Mishkin, Jack Clark, Gretchen Krueger, and Ilya Sutskever. Learning Transferable Visual Models From Natural Language Supervision, February 2021. URL <http://arxiv.org/abs/2103.00020>. arXiv:2103.00020 [cs].
- [24] Robin Rombach, Andreas Blattmann, Dominik Lorenz, Patrick Esser, and Björn Ommer. High-Resolution Image Synthesis with Latent Diffusion Models, April 2022. URL <http://arxiv.org/abs/2112.10752>. arXiv:2112.10752 [cs].
- [25] Martin Schrimpf, Jonas Kubilius, Ha Hong, Najib J. Majaj, Rishi Rajalingham, Elias B. Issa, Kohitij Kar, Pouya Bashivan, Jonathan Prescott-Roy, Kailyn Schmidt, Daniel L. K. Yamins, and James J. DiCarlo. Brain-Score: Which Artificial Neural Network for Object Recognition is most Brain-Like?, September 2018. URL <https://www.biorxiv.org/content/10.1101/407007v1>. Pages: 407007 Section: New Results.
- [26] Ghislain St-Yves, Emily J. Allen, Yihan Wu, Kendrick Kay, and Thomas Naselaris. Brain-optimized neural networks learn non-hierarchical models of representation in human visual cortex, January 2022. URL <https://www.biorxiv.org/content/10.1101/2022.01.21.477293v1>. Pages: 2022.01.21.477293 Section: New Results.
- [27] Yu Takagi and Shinji Nishimoto. High-resolution image reconstruction with latent diffusion models from human brain activity, November 2022. URL <https://www.biorxiv.org/content/10.1101/2022.11.18.517004v1>. Pages: 2022.11.18.517004 Section: New Results.
- [28] D. C. Van Essen, K. Ugurbil, E. Auerbach, D. Barch, T. E. J. Behrens, R. Bucholz, A. Chang, L. Chen, M. Corbetta, S. W. Curtiss, S. Della Penna, D. Feinberg, M. F. Glasser, N. Harel, A. C. Heath, L. Larson-Prior, D. Marcus, G. Michalareas, S. Moeller, R. Oostenveld, S. E. Petersen, F. Prior, B. L. Schlaggar, S. M. Smith, A. Z. Snyder, J. Xu, E. Yacoub, and WU-Minn HCP

- Consortium. The Human Connectome Project: a data acquisition perspective. *NeuroImage*, 62 (4):2222–2231, October 2012. ISSN 1095-9572. doi: 10.1016/j.neuroimage.2012.02.018.
- [29] Haiguang Wen, Junxing Shi, Yizhen Zhang, Kun-Han Lu, Jiayue Cao, and Zhongming Liu. Neural Encoding and Decoding with Deep Learning for Dynamic Natural Vision. *Cerebral Cortex*, 28(12):4136–4160, December 2018. ISSN 1047-3211, 1460-2199. doi: 10.1093/cercor/bhx268. URL <https://academic.oup.com/cercor/article/28/12/4136/4560155>.
- [30] Konstantin F. Willeke, Paul G. Fahey, Mohammad Bashiri, Laura Pede, Max F. Burg, Christoph Blessing, Santiago A. Cadena, Zhiwei Ding, Konstantin-Klemens Lurz, Kayla Ponder, Taliah Muhammad, Saumil S. Patel, Alexander S. Ecker, Andreas S. Tolias, and Fabian H. Sinz. The Sensorium competition on predicting large-scale mouse primary visual cortex activity, June 2022. URL <http://arxiv.org/abs/2206.08666>. arXiv:2206.08666 [cs, q-bio].
- [31] Mitchell Wortsman, Gabriel Ilharco, Samir Yitzhak Gadre, Rebecca Roelofs, Raphael Gontijo-Lopes, Ari S. Morcos, Hongseok Namkoong, Ali Farhadi, Yair Carmon, Simon Kornblith, and Ludwig Schmidt. Model soups: averaging weights of multiple fine-tuned models improves accuracy without increasing inference time, July 2022. URL <http://arxiv.org/abs/2203.05482>. arXiv:2203.05482 [cs].
- [32] Juntang Zhuang, Tommy Tang, Yifan Ding, Sekhar Tatikonda, Nicha Dvornek, Xenophon Papademetris, and James S. Duncan. AdaBelief Optimizer: Adapting Stepsizes by the Belief in Observed Gradients, December 2020. URL <http://arxiv.org/abs/2010.07468>. arXiv:2010.07468 [cs, stat].